International Journal of Steel Structures (2022) 22(6):1808–1816
https://doi.org/10.1007/s13296-022-00660-9

Online ISSN 2093-6311
Print ISSN 1598-2351

# Effect of UHPFRC Overlay on Fatigue Cracks Propagating from U-rib Welds of Orthotropic Steel Decks

**Masafumi Hattori**[1,2] · **Kazuo Tateishi**[2] · **Takeshi Hanji**[2] · **Masaru Shimizu**[2]

Received: 13 December 2021 / Accepted: 23 August 2022 / Published online: 6 September 2022


**Abstract**
Over the last decade, fatigue cracks have been observed at welded joints between U-ribs and deck plates in many orthotropic steel deck bridges in Japan. This paper focuses on fatigue cracks that initiate from a weld root of rib-to-deck welded joints and propagate to a deck plate. This study examines the effect of a countermeasure that uses overlaying Ultra-High Performance Fiber Reinforced cement-based Composites (UHPFRCs) on steel decks with cracks from U-rib welds, and confirms the fatigue durability of this method. Specifically, the retardation of crack propagation and the fatigue durability of the UHPFRC itself as well as the interface between the UHPFRC and the deck plate were confirmed by a wheel running test and finite element analysis. Based on the results, it was clarified that this countermeasure has a positive effect on retarding further crack propagation compared with the method of overlaying steel fiber reinforced concrete, which is generally adopted. In addition, it was revealed that the studied countermeasure has sufficient fatigue durability.

**Keywords** Orthotropic steel deck · Fatigue crack · UHPFRC overlay · Maintenance

## 1 Introduction

There have been reports of deck and bead propagation type cracks initiating from a weld root of rib-to-deck welded joints of orthotropic steel decks. These cracks may cause unevenness in the road surface and impede the safe passage of vehicles, so countermeasures are urgently required.

In general, countermeasures for these cracks include plate patching, welding repair, replacement of members, and change of pavement material. Considering the large scope of these methods and the necessity of preventive maintenance, reinforcement by changing the pavement material is considered to be a reasonable choice.

Reinforcement by changing the pavement material is a method in which the conventional asphalt pavement is changed to a pavement material with higher stiffness and lower temperature dependence of the modulus of elasticity in order to suppress the local deformation of the deck plate, which is one of the causes of fatigue cracks in the weld root of rib-to-deck welded joints of orthotropic steel deck. In previous studies, cement-based materials have been mainly considered as pavement materials, and many studies have focused on steel fiber reinforced concrete (SFRC) in particular (Inokuchi et al., 2010; Murakoshi et al., 2012; Ono et al., 2005a, 2005b; Walter et al., 2007).

In the case of SFRC laying, it is common to apply crack treatment to the cracks before laying. On the other hand, for deck propagation type cracks, it has been shown that under some conditions, such as when the crack size is sufficiently small, SFRC laying alone can retard crack growth without crack treatment (Murakoshi et al., 2012). The combination of appropriate inspection methods and countermeasures using paving materials can lead to a maintenance scenario that omits crack treatment, which in turn can lead to rationalization of maintenance management. Considering the expanded applicability of this maintenance scenario, it is desirable to apply a bedding material that can tolerate a wider range of crack sizes than SFRC.

The stress at the crack tip of a deck propagation type crack is expected to be reduced by the higher modulus of elasticity of the bedding material. In addition, Ultra-High

✉ Masafumi Hattori
m.hattori.ab@ri-nexco.co.jp

[1] Road Research Department, Nippon Expressway Research Institute Co. Ltd., 1-4-1 Tadao, Machida-shi, Tokyo 194-8508, Japan

[2] Department of Civil and Environmental Engineering, Nagoya University, Furo-cho, Chikusa-ku, Nagoya, Aichi 464-8603, Japan

Performance Fiber Reinforced cement-based Composites (UHPFRCs) are being developed as a material that has a higher modulus of elasticity than SFRC and can be installed in the field with the same construction machinery as SFRC. Based on the above, UHPFRCs may be more suitable than SFRC as a laying material in the maintenance scenario without crack treatment. There have been several studies on composite structures using UHPFRCs and pavement materials with similar material properties laid on orthotropic steel deck (Dieng et al., 2013; Liu et al., 2019; Shao et al., 2013). However, the effect of UHPFRC laying on the retardation of deck propagating crack growth and the durability of the countermeasure itself have not been fully clarified.

The purpose of this study is to clarify the effect of UHPFRC laying on the retardation of deck propagation type crack growth and to confirm the fatigue durability of the countermeasure itself at the weld between the U-rib and the deck plate of the existing orthotropic steel deck, which usually has relatively thin deck plate. Specifically, fatigue tests and finite element analyses were conducted to investigate the propagation of deck propagation type cracks and stress intensity factors before and after the countermeasure, as well as the fatigue durability of the laid material and the interface with the deck plate. The countermeasure effect of UHPFRC laying was clarified in comparison with the commonly used SFRC laying. The fatigue tests were conducted using wheel running tests with rubber tires in order to approximate the loading conditions of the actual bridge.

## 2 Outline of Wheel Running Test

The specimen is a partial model of an orthotropic steel deck bridge with three cross ribs and three U-ribs, as shown in Fig. 1. By analytically comparing the local stress behavior of one panel of an orthotropic steel deck bridge and the test specimen, it is confirmed that the partial model is able to reproduce the real bridge. In the following, the section name is defined as shown in Fig. 1 (e.g. Sec. A, Line 1). The weld penetration depth of rib-to-deck welded joint is 83.7% of the U-rib thickness and the weld leg length is 7.3 mm on the deck plate side and 6.9 mm on the U-rib side in Sec. G. The specimen is fixed to the support frame at the position shown by the green box in Fig. 1.

After applying the epoxy resin adhesive on the deck plate, UHPFRC is overlaid with a thickness of 40 mm. The elastic modulus of the UHPFRC was 44.1 kN/mm$^2$ at the start of the test. Bolted joints and UHPFRC construction joints that are thought to affect fatigue durability are provided within the load running area. In addition, the bolted joints were smoothed with resin mortar and coated with adhesive before overlaying the UHPFRC.

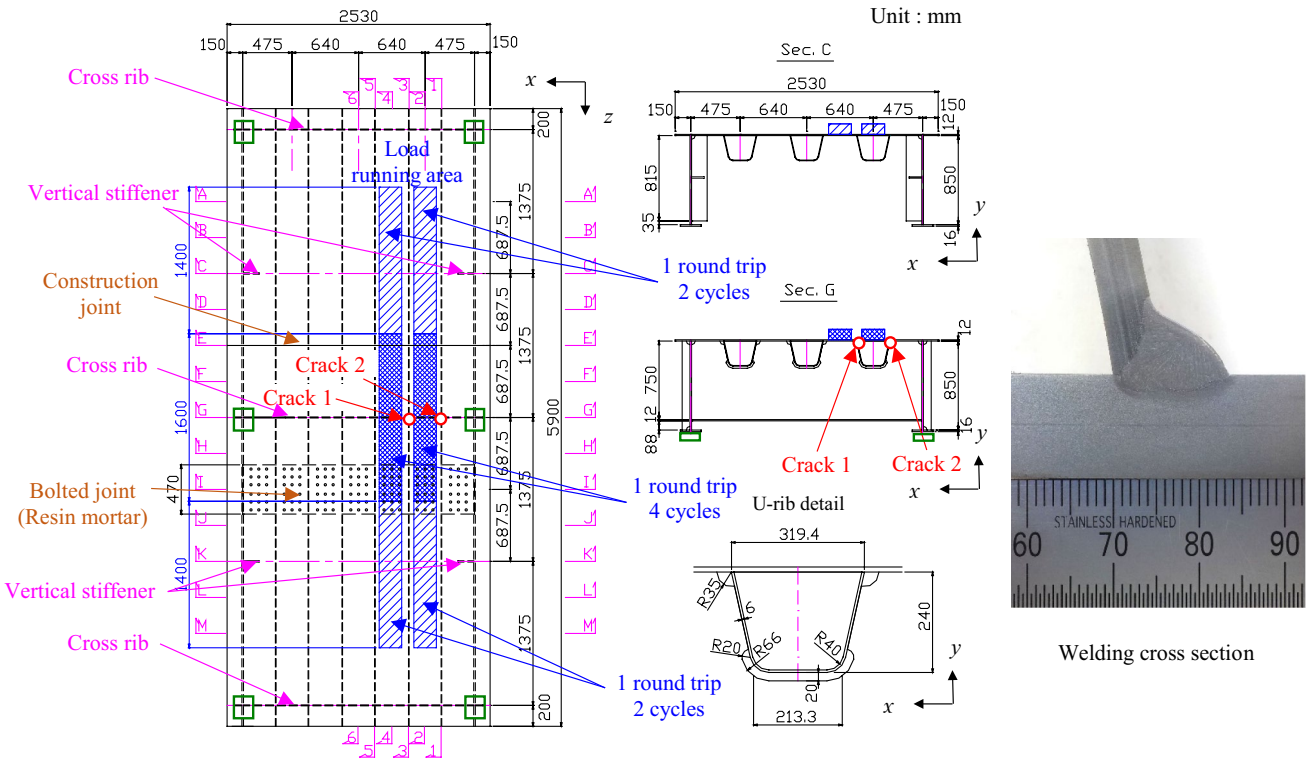


**Fig. 1** Specimen

Figure 2 shows the wheel running machine. A loading trolley with tandem shaft double tires makes 6 round trips per minute over 3 m range. The machine is installed outdoors. The load running area is the part of the blue hatch shown in Fig. 1, so that the center of the double tire passes through Line 3. The weight of trolley is 140 kN, assuming a legal load (including impact effects) in Japan.

The test was conducted according to the following flow.

*Step 1* Fatigue test with only orthotropic steel deck (1.26 million cycles) and introducing two fatigue cracks (Crack 1, 2 as shown in Fig. 1).
*Step 2* Overlaying UHPFRC without crack treatment.
*Step 3* Fatigue test in natural environment after UHPFRC overlay (1.02 million cycles).
*Step 4* Fatigue test in water-filled state after UHPFRC overlay (1.01 million cycles).
*Step 5* UHPFRC adhesion test.
*Step 6* Observing the fracture surface of the cracks.

Step 1 was conducted to introduce deck propagation type cracks into the specimen. The loading was terminated at 1.26 million cycles when the crack depth of Crack 2, estimated by ultrasonic testing, exceeded 10 mm. After that, a dye-marking was left on the crack surface by spraying blue varnish around the crack from the inner surface of the U-rib in order to record the crack sizes at the timing of the UHPFRC laying.

In Step 2, UHPFRC was laid on the top of the deck plate with the crack in place without crack treatment. In the construction, the bolted joints were smoothed with a resin mortar repair material. After that, adhesive was applied and the UHPFRC was laid. The laying was carried out over 2 days, and the construction joints were introduced into the specimens.

Steps 3 and 4 were conducted to apply cyclic loading by wheel load running to the existing cracks, UHPFRC and its interface with the deck plate. In Step 3, the test specimen was loaded 1.02 million cycles under the same conditions as in Step 1. Since the wheel load traveling test machine used in this study was installed outdoors, this is referred to as a test under natural environmental conditions. In Step 4, the test was continued in a water-filled condition where the UHPFRC was immersed in water. The water-filled condition was created by pooling such that the edges of the UHPFRC were flooded as shown in Fig. 3.

Step 5 was conducted to check the residual adhesion strength between the UHPFRC and the deck plate. The adhesion test was carried out by drilling a core with a diameter of 80 mm from the top of the UHPFRC to the deck plate, and applying a tensile load to a pull-out jig bonded to the top of the core.

In Step 6, macro-fracture surface observation was conducted to confirm the propagation of the existing cracks. Cross-sectional observations were also made by cutting the specimen at the point where the crack depth was the deepest.

## 3 Outline of Finite Element Analysis

FE analysis was conducted to confirm the effect of reducing the stress intensity factor by UHPFRC overlay. The analysis model is shown in Fig. 4. The analysis program used is Abaqus 6.14. The analysis is performed using a global model and submodels, and the submodels are driven based on the displacements of the global model. The elements were based

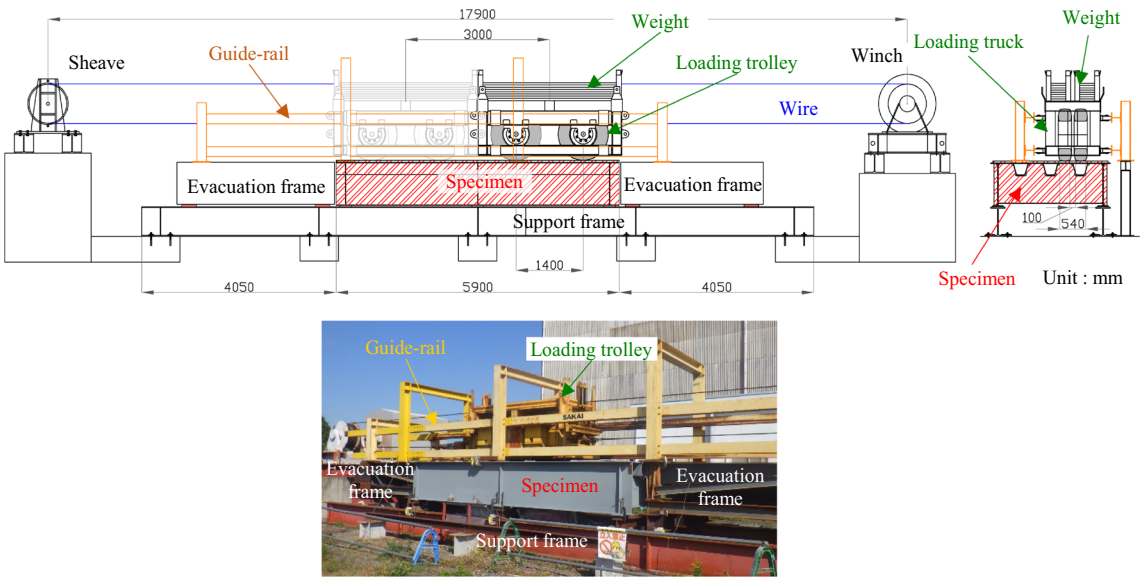


**Fig. 2** Wheel running machine

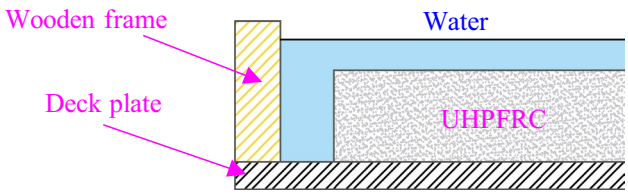


**Fig. 3** Water-filled condition at the edge of the UHPFRC

on linear 3D 8-node solid elements. The dimensions of the global model are the same as those of the specimen. As boundary conditions, the bottom surface of the lower flanges shown with green boxes in Fig. 1 were completely fixed. The weld bead and root are created in the submodels. The weld leg length is 6 mm and the penetration depth is 75% (4.5 mm) of the U-rib thickness. Although the penetration depth differs between the experiment and the analysis, the effect of this difference on the stress properties of the root is considered to be small (Hattori et al., 2021). Semi-elliptical

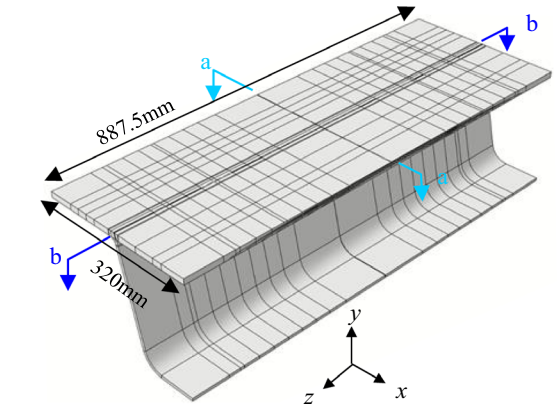


| | Nurber of elements | Nurber of nodes | |
|---|---|---|---|
| | | $a$=1 | $a$=11 |
| No reinforcement | 382,504 | 382,504 | 390,959 |
| Reinforcement | 452,260 | 459,574 | 463,389 |

Submodel 2 (Sec. C)

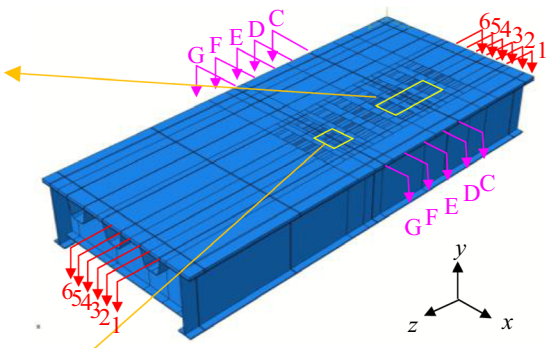


| | Nurber of elements | Nurber of nodes |
|---|---|---|
| No reinforcement | 296,209 | 397,999 |
| Reinforcement | 855,755 | 974,159 |

Global model

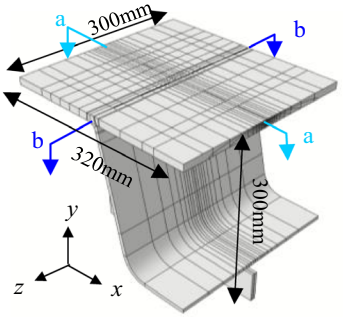


| | Nurber of elements | Nurber of nodes | |
|---|---|---|---|
| | | $a$=1 | $a$=11 |
| No reinforcement | 176,900 | 172,442 | 174,283 |
| Reinforcement | 195,410 | 192,492 | 194,314 |

Submodel 1 (Sec. G)

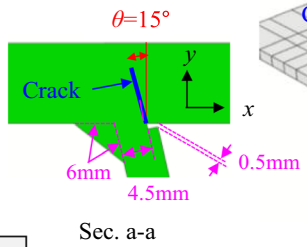


Sec. a-a

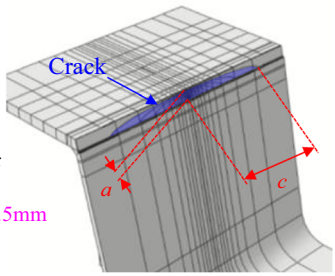


Sec. b-b

Crack size

Sub model 1 Unit: mm

| | | | | | | | | | | | |
|---|---|---|---|---|---|---|---|---|---|---|---|
| $a$ | 1 | 2 | 3 | 4 | 5 | 6 | 7 | 8 | 9 | 10 | 11 |
| $c$ | 2 | 4 | 7 | 10 | 14 | 19 | 26 | 35 | 48 | 69 | 108 |

Sub model 2

| | | | | | | | | | | | |
|---|---|---|---|---|---|---|---|---|---|---|---|
| $a$ | 1 | 2 | 3 | 4 | 5 | 6 | 7 | 8 | 9 | 10 | 11 |
| $c$ | 32.5 | 65 | 97.5 | 130 | 162.5 | 195 | 227.5 | 260 | 292.5 | 325 | 357.5 |

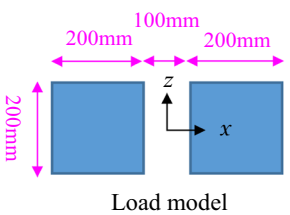


Load model

**Fig. 4** Finite element analysis model

cracks are introduced in the submodels by double nodes as shown Fig. 4. Since no crack was introduced in the global model, the submodeled area was considered to be enough large so that the displacement at the boundary between the global model and submodel is not affected by existence of a crack. In this study, crack closure and welding residual stress are not considered. The crack shape is based on previously reported deck propagation type cracks (Kainuma et al., 2016; Ono et al., 2005a, 2005b, 2009). The crack size is determined by referring to the literature (Kainuma et al., 2017; Murakoshi et al., 2019), which is larger than the cracks obtained in this experiment and can provide a conservative consideration. The element size around the crack front used to calculate the stress intensity factor is $0.1 \times 0.1 \times 0.1$ mm.

Table 1 shows the analysis cases. There are three cases: no reinforcement, UHPFRC overlay, and SFRC overlay for comparison. Since there is a possibility that the adhesive may not work well, the analysis cases are also created without an adhesive. The no-adhesion condition was simulated by making the elastic modulus of the adhesive extremely small.

The load model is created with reference to the load for fatigue design of Japanese road bridges. Specifically, we assume a double tire shape in which a loading area of $200 \times 200$ mm is arranged at intervals of 100 mm as shown in Fig. 4, and 140 kN is loaded there.

**Table 1** Analysis cases

| Analysis case | Name | Deck plate | | | Adhesive | | | Laying material | | |
|---|---|---|---|---|---|---|---|---|---|---|
| | | Thickness (mm) | Elastic modulus (kN/mm$^2$) | Poisson's ratio | Thickness (mm) | Elastic modulus (kN/mm$^2$) | Poisson's ratio | Thickness (mm) | Elastic modulus (kN/mm$^2$) | Poisson's ratio |
| No reinforcement | NR | 12 | 206 | 0.3 | – | | | – | | |
| UHPFRC | UH-B | | | | 1 | 2 | 0.2 | 40 | 45 | 0.2 |
| | UH-N | | | | | 0.01 | | | | |
| SFRC | SF-B | | | | | 2 | | | 33 | |
| | SF-N | | | | | 0.01 | | | | |

## 4 Effect of Retarding Crack Propagation with UHPFRC Overlaying

In order to clarify the retarding effect on crack propagation by overlaying UHPFRC, the fracture surface observation and crack propagation behavior obtained by the wheel running test and the relationship between stress intensity factor and crack depth obtained by FE analysis were considered.

### 4.1 Fracture Surface Observation

From the macro fracture surface observed in Step 6, the crack surfaces were semi-elliptical centered on the cross rib section. The crack sizes were $2c = 58$ mm and $a = 7.0$ mm for Crack 1, and $2c = 88$ mm and $a = 8.7$ mm for Crack 2. Here, $c$ is the half crack length, and $a$ is the crack depth. The crack surface was dye-marked with blue varnish after the completion of Step 1, and it was confirmed in Step 6 that the fatigue fracture surface and the surface colored in blue coincide. In other words, it can be confirmed that there was no crack propagation after the UHPFRC was overlaid.

### 4.2 Relationship Between Stress Intensity Factor and Crack Depth

Figure 5 shows the relationship between the stress intensity factor $K$ and the crack depth $a$ when loaded on Submodel 2 of Sec. C in analysis case NR. The deformation mode of the crack is defined as shown in Fig. 6. The displacement indicated by the arrow is the positive, and the opposite is the negative. It is noted that the analysis can give the negative value to $K_I$ because it does not take into account the crack surface contact. The fracture angle $\theta_f$ is the angle at which the energy release rate at the crack tip is maximized, and was calculated from Eq. 1 (Chang et al., 2006).

$$\frac{1-\nu}{2}\left\{K_I^2\left(\sin\frac{\theta_f}{2}+\sin\frac{3\theta_f}{2}\right)+4K_IK_{II}\cos\frac{3\theta_f}{2}-K_{II}^2\left(3\sin\frac{3\theta_f}{2}-5\sin\frac{\theta_f}{2}\right)\right\}+K_{III}^2\sin\frac{\theta_f}{2}=0 \quad (1)$$

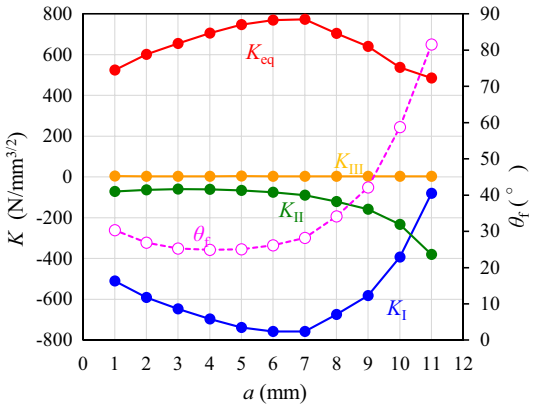


**Fig. 5** The relationship between the stress intensity factor and the crack depth when loaded on Sec. C

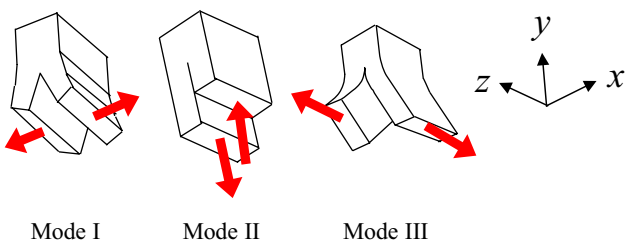


**Fig. 6** Definition of crack deformation mode

here $\nu$ is Poisson's ratio and the subscripts I, II, and III represent deformation modes of the crack tip. The equivalent stress intensity factor $K_{eq}$ is the stress intensity factor corresponding to mode I for cracks in the same direction as the fracture angle, and can be calculated from Eq. 2 (Chang et al., 2006).

$$K_{eq}=\left[\frac{1}{1-\nu}\cos^2\frac{\theta_f}{2}\left\{\frac{1-\nu}{2}\left(K_I^2\left(1+\cos\theta_f\right)-4K_IK_{II}\sin\theta_f+K_{II}^2\left(5-3\cos\theta_f\right)\right)+K_{III}^2\right\}\right]^{\frac{1}{2}} \quad (2)$$

From Fig. 5, the absolute value of $K_I$ is almost the same as $K_{eq}$ in the range of $a/t = 1/6$ to $5/6$ ($t$: deck plate thickness), and it can be said that mode I is dominant in the deck propagation type crack in this range. Based on the above, we will consider only mode I in the following.

$K_I$ has an extremum near $a = 6$–$7$ mm. In other words, after the crack reaches a size of $a/t = 1/2$–$7/12$, the stress intensity factor decreases with the subsequent propagate, so it is possible to arrest propagation of the remaining cracks depending on the countermeasure method. On the other hand, there is a concern about new crack formation from the upper surface of the deck plate due to the reduction of the ligament, but this crack formation can be prevented because the stress at the ligament can be reduced by the countermeasures.

### 4.3 Crack Propagation Behavior

Figure 7 shows a cross-sectional photograph of the deepest part of Crack 1 observed in Step 6. The figure also shows the crack propagation curve obtained by the analysis assuming that the crack propagates in the direction of the fracture angle $\theta_f$. In terms of the crack path, the angle is large at a small stage of the crack, decreases as the crack propagates,

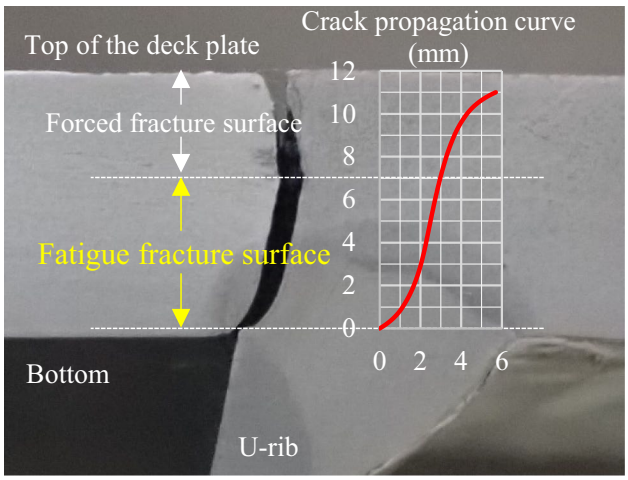


**Fig. 7** A cross-sectional photograph of the deepest part of Crack 1

and increases again as the crack propagates. The behavior of the change is almost consistent with that of the crack propagation curve obtained from elastic finite element analysis, which does not take into account crack closure and welding residual stress. In other words, the crack propagation behavior can be simulated to some extent by the analysis method in this study.

### 4.4 Stress Intensity Factor Range

The relationship between the stress intensity factor range and the crack depth was determined for different overlaying materials. Figure 7 shows the relationship between the stress intensity factor range and the crack depth when loaded on Sec. C. Here, we assume a double tire shape in which a loading area of 220 × 235 mm is arranged at intervals of 100 mm as shown in Fig. 2, and 70 kN is loaded there. As an overall tendency, $\Delta K_I$ becomes smaller in the order of analysis cases UH-B, SF-B, UH-N, SF-N, and NR. The difference in $\Delta K_I$ between the UHPFRC and SFRC is smaller than that between with and without adhesive. In other words, the durability of the adhesive, which is responsible for the composite function, is considered to be important.

Figure 8 also shows the threshold stress intensity factor range $\Delta K_{th} = 63$ N/mm$^{3/2}$ (JSSC, 2012). $\Delta K_I$ is about the same as $\Delta K_{th}$ in the case UH-B at about $a = 4$ mm and in the case SF-B at about $a = 1$ mm. If crack arrest can be evaluated by $\Delta K_{th}$, in the case of the UHPFRC, there is a possibility that the crack depth that is arrested can be increased by about 3 mm compared to SFRC. In other words, it is inferred that the UHPFRC overlay is superior to the SFRC overlay in the maintenance scenario without crack treatment.

The stress intensity factor ranges calculated for the cracks from the wheel load tests (see in Sect. 4.1) were 51.1 N/mm$^{3/2}$ for Crack 1 and 118.4 N/mm$^{3/2}$ for Crack 2, respectively. In other words, the cracks could be arrested at least up to $\Delta K_I = 118.4$ N/mm$^{3/2}$. Therefore, the evaluation by $\Delta K_{th}$ is considered to be conservative.

## 5 Fatigue Durability of UHPFRC Overlaying

The fatigue durability of UHPFRC itself and the interface between UHPFRC and the deck plate was clarified in Step 3 and 4 in the wheel running test.

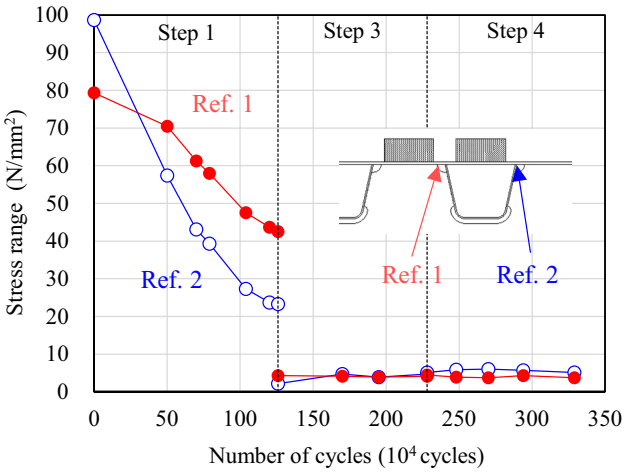


**Fig. 9** The relationship between the fluctuation range of stress at a reference point 5 mm away from the weld toe and the number of cumulative loads during the wheel load running test

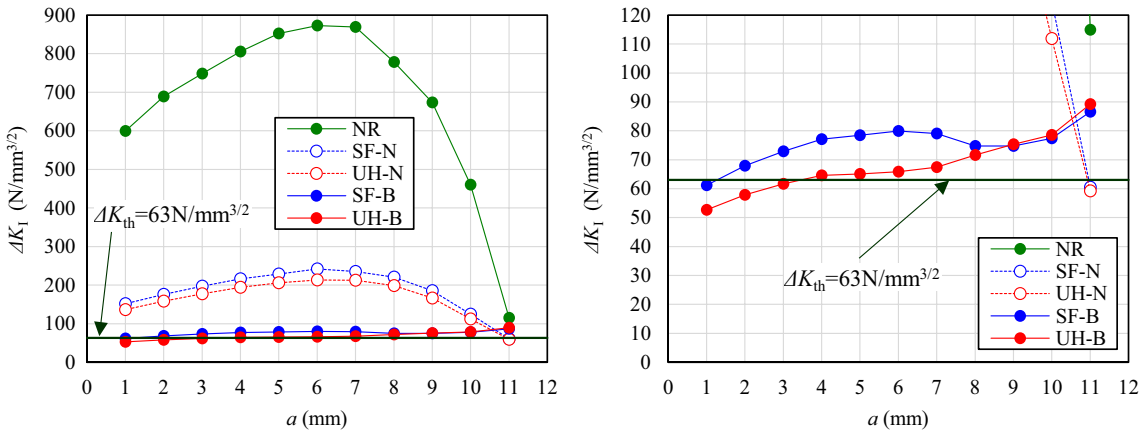


**Fig. 8** The relationship between the stress intensity factor range and the crack depth when loaded on Sec. C (The vertical axis in the left graph is expanded in the right graph)

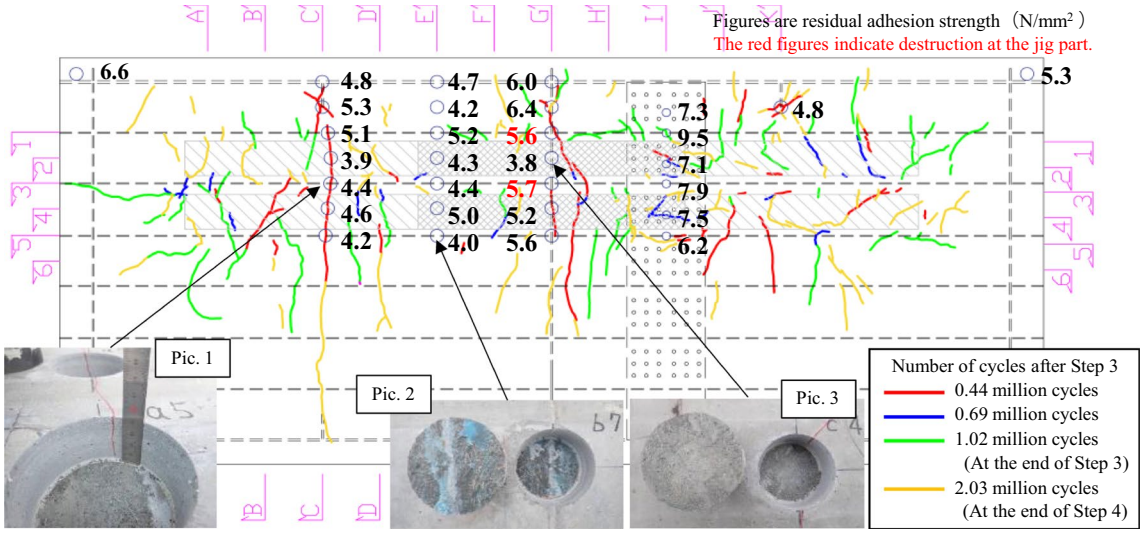


**Fig. 10** The cracks on the top surface of the UHPFRC and the residual adhesion strength between the UHPFRC and the deck plate

### 5.1 Relationship Between Stress Range Near the Weld and the Number of Cycles

Figure 9 shows the relationship between the fluctuation range of stress at a reference point 5 mm away from the weld toe and the number of cumulative loads during the wheel load running test. In Step 1, Crack 1 and 2 were confirmed near Ref. 1 and 2, these were considered that the stress range had been decreased as the crack propagation. On the other hand, there are almost no changes in the stress range during Step 3 and 4. From this, it is presumed that there is no deterioration of the UHPFRC itself and the interface between the UHPFRC and the deck plate due to repeated loading, at least near the stress measurement point.

### 5.2 Cracks on the Surface of the UHPFRC

The cracks on the top surface of the UHPFRC are shown in Fig. 10. When loading 0.44 million cycles in Step 3, cracks in the transverse direction were confirmed in Sec. C, G, and K. After that, the crack density increased around the load running area as the number of cycles increased. However, the maximum crack width at the end of Step 4 was 0.08 mm, and it is presumed that the crack width did not become large due to the crack dispersibility of UHPFRC. In addition, there was no noticeable damage on the bolted joints and UHPFRC construction joints. The results of core drilling at the location with the largest crack width are shown in Pic. 1 in Fig. 10. Cracks that reach the deck plate can be seen, but they are so fine that they can only be seen by applying acetone. Although the opening width of the UHPFRC construction joints was at most 0.3 mm, it was already open at the start of the test. Therefore, the main cause of opening was material shrinkage, and the effect of cyclic loading was considered to be small.

### 5.3 Residual Adhesion Strength Between the UHPFRC and Deck Plate

The residual adhesion strength between the UHPFRC and the deck plate determined from the adhesion test is shown in Fig. 10. After Step 4, the residual adhesion strength between the UHPFRC and the deck plate was investigated by adhesion tests of 30 locations. Adhesion tests were conducted by drilling a core from the UHPFRC up to the deck plate and then pulling it out vertically. The residual adhesion strength is the maximum load in the adhesion test divided by the cross-sectional area of the core. The test points were Sec. C, which had the maximum crack width, Sec. E, which had UHPFRC construction joints, Sec. G, which was on cross rib section, and Sec. I, which had bolted joints. A residual adhesion strength with an average of 5.0 N/mm$^2$ and a standard deviation of 0.8 N/mm$^2$ was confirmed in the results. The maximum stress acting on the adhesive obtained from FE analysis is 2.4 N/mm$^2$, and it is considered that sufficient adhesiveness can be obtained.

## 6 Conclusions

This study aimed to clarify the effect of UHPFRC laying on the retardation of deck propagation type crack growth and to confirm the fatigue durability of the countermeasure

itself at the weld between the U-rib and the deck plate of the orthotropic steel deck. For this purpose, wheel running tests and finite element analysis were conducted. The main results obtained are shown below.

(1) For two deck propagation type cracks obtained by wheel running tests, it was confirmed that the propagation of the cracks could be retarded by UHPFRC overlay without crack treatment. It was also shown that the crack propagation trends could be roughly evaluated by elastic finite element analysis, which does not take into account the crack closure and welding residual stress.
(2) It is clear that Mode I is dominant for the propagation of cracks, at least in the range of crack depths from 1/6 to 5/6 of the deck plate thickness. The stress intensity factor of Mode I reached its extreme value when the crack depth was 1/2–7/12 of the deck plate thickness, and then decreased with the progress of the crack.
(3) The difference between the UHPFRC and the SFRC overlay in the stress intensity factor range of deck propagating cracks was smaller than the difference between overlaid materials with and without adhesion to the deck plate. In other words, the durability of the adhesive is more important than the stiffness of the overlaid material.
(4) It was shown that there is a difference of about 3 mm in the crack depth within the same stress intensity factor range between UHPFRC and SFRC. In the case of UHPFRC, there is a possibility that the arresting crack depth can be increased by about 3 mm compared with that of SFRC, and it is inferred that UHPFRC is superior to SFRC in the maintenance scenario without crack treatment.
(5) The wheel running test confirmed that there was no significant degradation of the UHPFRC material itself or its interface with the deck plate, indicating that the UHPFRC laying had sufficient fatigue resistance.

## References


Chang, J., Xi, J., & Mutoh, Y. (2006). A general mixed-mode brittle fracture criterion for cracked materials. *Engineering Fracture Mechanics, 73*, 1249–1263.

Dieng, L., Marchand, P., Gomes, F., Tessier, C., & Toutlemonde, F. (2013). Use of UHPFRC overlay to reduce stress in orthotropic steel decks. *Journal of Constructional Steel Research, 89*, 30–41.

Hattori, M., Tateishi, K., Hanji, T., & Shimizu, M. (2021). Fatigue evaluation for root cracks in U-rib to deck welded joints of orthotropic steel decks. *Journal of Japan Society of Civil Engineers, 77*(2), 255–270 (**in Japanese**).

Inokuchi, S., Ishii, H., Ishigaki, T., Maeno, H., Sumi, T., & Yamada, K. (2010). Fatigue assessment for weld between deck plate and U-rib in orthotropic steel decks with consideration of pavement properties. *Journal of Japan Society of Civil Engineers, 66*(1), 79–91 (**in Japanese**).

Japanese Society of Steel Construction. (2012). *Fatigue design recommendations for steel structure*. Tokyo, Gihodo Shuppan, (in Japanese)

Kainuma, S., Yang, M., Jeong, Y., Inokuchi, S., Kawabata, A., & Uchida, D. (2016). Experiment on fatigue behavior of rib-to-deck weld root in orthotropic steel decks. *Journal of Constructional Steel Research, 119*, 113–122.

Kainuma, S., Yang, M., Jeong, Y., Inokuchi, S., Kawabata, A., & Uchida, D. (2017). Experimental investigation for structural parameter effects on fatigue behavior on rib-to-deck welded joints in orthotropic steel decks. *Engineering Failure Analysis, 79*, 520–537.

Liu, Y., Zhang, Q., Meng, W., Bao, Y., & Bu, Y. (2019). Transverse fatigue behavior of steel-UHPC composite deck with large-size U-ribs. *Engineering Structures, 180*, 388–399.

Murakoshi, J., Kosuge, T., Ishii, H., Kasugai, T., Toyama, N., & Ishizawa, T. (2012). Study on retrofit effect by SFRC overlay for existing orthotropic steel deck with fatigue crack through rib-to-deck weld. *Journal of Japan Society of Civil Engineers, A1, 68*(3), 722–737. (**in Japanese**).

Murakoshi, J., Mori, T., Haba, S., Ono, S., Sato, A., & Mori, T. (2019). Retrofit effect of SFRC overlay on fatigue durability of orthotropic steel decks with cracks extending to deck plate. *Journal of Japan Society of Civil Engineers, A1, 75*(2), 194–205 (**in Japanese**).

Ono, S., Shimozato, T., Inaba, N. & Miki, C. (2005a). Wheel running fatigue test for orthotropic steel bridge decks. In *Proceeding of 58th IIW Annual Assembly*, XIII-2070-05.

Ono, S., Hirabayashi, Y., Shimozato, T., Inaba, N., Murano, M., & Miki, C. (2009). Fatigue properties and retrofitting of existing orthotropic steel bridge decks. *Journal of Japan Society of Civil Engineers, 65*(2), 335–347 (**in Japanese**).

Ono, S., Shimozato, T., Masui, T., Machida, F., & Miki, C. (2005b). Retrofitting method for existing orthotropic steel deck. *Journal of Japan Society of Civil Engineers, 801*(73), 213–226 (**in Japanese**).

Shao, X., Yi, D., Huang, Z., Zhao, H., Chen, B., & Liu, M. (2013). Basic performance of the composite deck system composed of orthotropic steel deck and ultrathin RPC layer. *Journal of Bridge Engineering, 18*(5), 417–428.

Walter, R., Olesen, J. F., Stang, H., & Vejrum, T. (2007). Analysis of an orthotropic deck stiffened with a cement-based overlay. *Journal of Bridge Engineering, 12*(3), 350–363.